JOURNAL OF THE ROYAL SOCIETY Interface

Preload-responsive adhesion: effects of aspect ratio, tip shape and alignment

Dadhichi Paretkar, Marleen Kamperman, David Martina, Jiahua Zhao, Costantino Creton, Anke Lindner, Anand Jagota, Robert McMeeking and Eduard Arzt

J. R. Soc. Interface 2013 **10**, 20130171, published 3 April 2013

JOURNAL OF THE ROYAL SOCIETY Interface

rsif.royalsocietypublishing.org

Research

Cite this article: Paretkar D, Kamperman M, Martina D, Zhao J, Creton C, Lindner A, Jagota A, McMeeking R, Arzt E. 2013 Preload-responsive adhesion: effects of aspect ratio, tip shape and alignment. J R Soc Interface 10: 20130171.
http://dx.doi.org/10.1098/rsif.2013.0171

Received: 22 February 2013
Accepted: 8 March 2013

Subject Areas:
biomimetics

Keywords:
dry adhesion, responsive, bioinspired

Authors for correspondence:
Dadhichi Paretkar
e-mail: dadhichi.paretkar@inm-gmbh.de
Eduard Arzt
e-mail: eduard.arzt@inm-gmbh.de

Electronic supplementary material is available at http://dx.doi.org/10.1098/rsif.2013.0171 or via http://rsif.royalsocietypublishing.org.

Royal Society Publishing
Informing the science of the future

Preload-responsive adhesion: effects of aspect ratio, tip shape and alignment

Dadhichi Paretkar[1,5], Marleen Kamperman[1,4], David Martina[2], Jiahua Zhao[1], Costantino Creton[2], Anke Lindner[3], Anand Jagota[1,5], Robert McMeeking[1,6,7] and Eduard Arzt[1]

[1]INM-Leibniz Institute for New Materials, Functional Surfaces Group, Saarland University, Campus D2 2, 66123 Saarbruecken, Germany
[2]Laboratoire PPMD, and [3]Laboratoire PMMH, ESPCI, 10 Rue Vauquelin, 75231 Paris Cédex 05, France
[4]Physical Chemistry and Colloid Science, Wageningen University, Dreijenplein 6, 6703 HB Wageningen, The Netherlands
[5]Department of Chemical Engineering, Lehigh University, Bethlehem, PA 18015, USA
[6]Department of Mechanical Engineering and Materials Department, University of California, Santa Barbara, CA 93106, USA
[7]School of Engineering, University of Aberdeen, King's College, Aberdeen AB24 3UE, UK

We tested the adhesive response of polymer surfaces structured with arrays of cylindrical fibrils having diameters of 10–20 μm and aspect ratios 1–2.4. Fibrils had two different tip shapes of end-flaps and round edges. A preload-induced mechanical buckling instability of the fibrils was used to switch between the states of adhesion and non-adhesion. Non-adhesion in fibrils with round edges was reached at preloads that caused fibril buckling, whereas fibrils with end-flaps showed adhesion loss only at very high preloads. The round edge acted as a circumferential flaw prohibiting smooth tip contact recovery leading to an adhesion loss. *In situ* observations showed that, after reversal of buckling, the end-flaps unfold and re-form contact under prevailing compressive stress, retaining adhesion in spite of buckling. At very high preloads, however, end-flaps are unable to re-form contact resulting in adhesion loss. Additionally, the end-flaps showed varying contact adaptability as a function of the fibril–probe alignment, which further affects the preload for adhesion loss. The combined influence of preload, tip shape and alignment on adhesion can be used to switch adhesion in bioinspired fibrillar arrays.

1. Introduction

Synthetic gecko-inspired adhesives rely on fibrillar structures that create non-chemical adhesion by concentrating intermolecular forces between two bodies, as discussed in recent reviews [1–3]. The potential to incorporate switchability in adhesion has only recently been explored. Examples include systems that respond to external stimuli such as temperature [4,5], magnetic field [6], mechanical deformation [7,8] and pneumatic pressure [9,10]. The common underlying principle is a reversible change in the area of contact between the adhesive surface and the test probe, leading to a change in adhesion.

In our previous work [8], the adhesion dependence on preload was established for polydimethylsiloxane (PDMS) fibrils with aspect ratio (AR) 3 (i.e. fibril height h divided by diameter d). Pull-off strengths at low preloads were high, whereas loss in adhesion was shown to occur at high preloads. The transition was due to a buckling instability of the fibrils at preloads higher than a critical value; it was also shown to be reversible and repeatable. Whenever the fibrils were unable to re-form an intimate contact with the probe, in spite of buckling reversal, adhesion was lost. At low preloads, however, the fibrils were able to re-form probe contact after buckling reversal. Thus, there is an important difference between the critical preload that causes buckling and the preload that causes adhesion loss.

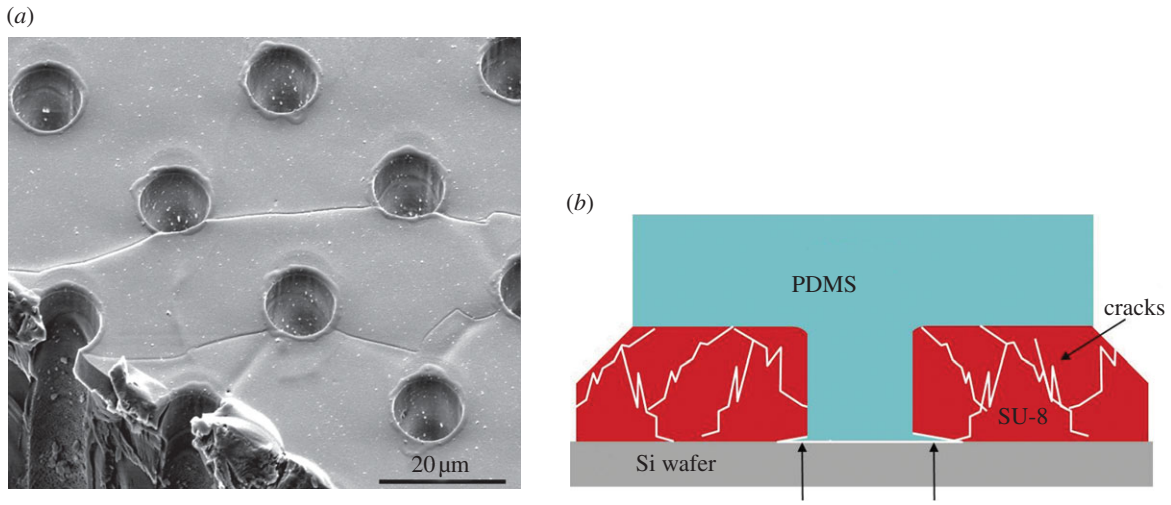

Figure 1. (*a*) Scanning electron micrograph of nanoscale cracks on the surface of a SU-8 resist film containing a hole pattern. (*b*) Schematic of a three-dimensional network of cracks in the resist film and delamination at the SU-8/Si wafer interface owing to thermal stresses. Liquid PDMS fills the hole and the holes and the gaps between the SU-8 film and the wafer (see arrows). (Online version in colour.)

Table 1. Dimensions of fibrils of both shapes for different aspect ratios (AR = h/d) and a schematic of the end-flap showing its thickness and width.

AR	pillar h, d type 1 (µm)	pillar h, d type 2 (µm)	width of end-flaps (nm)	thickness of end-flaps (nm)
1	20, 20	20, 20	360 ± 10	310 ± 40
1.4	20, 14	20, 14	565 ± 5	365 ± 35
2	20, 10	20, 10	1250 ± 50	635 ± 15
2.4	33, 14	27, 11	450 ± 5	340 ± 10

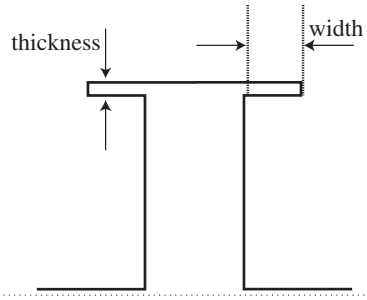

In the present paper, the mechanism of adhesion transition will be studied in more detail. First, the dependence of the critical preload that causes fibril mechanical instability on the fibril's AR will be established for different ARs (h/d) of 1–2.4, and diameters 10–20 µm. Second, the influence of tip shape on the adhesion transition will be investigated. Contact reformation during the reversible buckling will be compared for two different terminal contact shapes, namely end-flaps (denoted type 1) and round edges (type 2). Finally, practical considerations of using fibrillar arrays as switchable adhesives demand contact adaptability in non-aligned orientations. The effect of systematic changes in sample alignment with respect to a flat test probe on preload-dependent adhesion will be investigated here. Given this background, different ARs of type 1 and type 2 adhesives were tested for their performance by varying the applied preload and sample alignment. The focus throughout is on gaining understanding of switchable adhesion through study of mechanistic details.

2. Experimental methods

Photolithography and replica moulding techniques were used to structure PDMS (Sylgard 184, Dow Corning, MI, USA) surfaces with an array of hexagonally arranged micropillars. PDMS fibrils having four different ARs of 1, 1.4, 2 and 2.4, and diameters of 10, 14 and 20 µm were fabricated (table 1). Different diameters resulted from the sizes chosen for the circular patterns in the photomasks. The length of fibrils was governed by the thicknesses of the SU-8 films. SU-8 resists, i.e. SU-8 2010 and SU-8 2025 (Micro Resist Technology, Berlin, Germany), were spun to obtain desired thicknesses of 20, 27 and 33 µm. Table 1 summarizes the dimensions of the pillars (length, h and diameter, d) for four ARs of type 1 and type 2 fibrils on a PDMS backing having thickness in the range 2–2.5 mm.

2.1. Fabrication of micropillars with end-flaps: type 1 fibrils

Thermal-strain-mismatch-induced cracking of SU-8 films was used to generate end-flaps (similar to mushroom-heads) on fibrils following the previous work of del Campo *et al.* [11]. The photothermal cross-linking process in SU-8 is completed only after a post-exposure bake ($T = 95^{\circ}$C) [12]. Slow cooling after the bake is usually recommended to minimize the thermal stresses in the stiff, fully cross-linked SU-8. However, by placing the wafers directly on a cool steel surface ($T \sim 20^{\circ}$C) thermal stress was induced in the SU-8 film. The magnitude of the equi-biaxial thermal stress was estimated to be 19 MPa (SU-8 coefficient of thermal expansion (CTE) = 50 ppm K^{-1} and Si CTE = 2.6 ppm K^{-1}) [13]. Thermal stress caused the SU-8 film to crack and delaminate from the wafer at the base of the cylindrical holes (figure 1*b*).

Cracks/gaps present in the SU-8 film (figure 1*a*), which have feature sizes of several tens of nanometres, are replicated in the PDMS structure owing to its high fidelity to the mould [14]. During the soft-moulding procedure, the uncross-linked liquid PDMS filled the lithographic holes in the SU-8 master as well as the submicrometre delamination

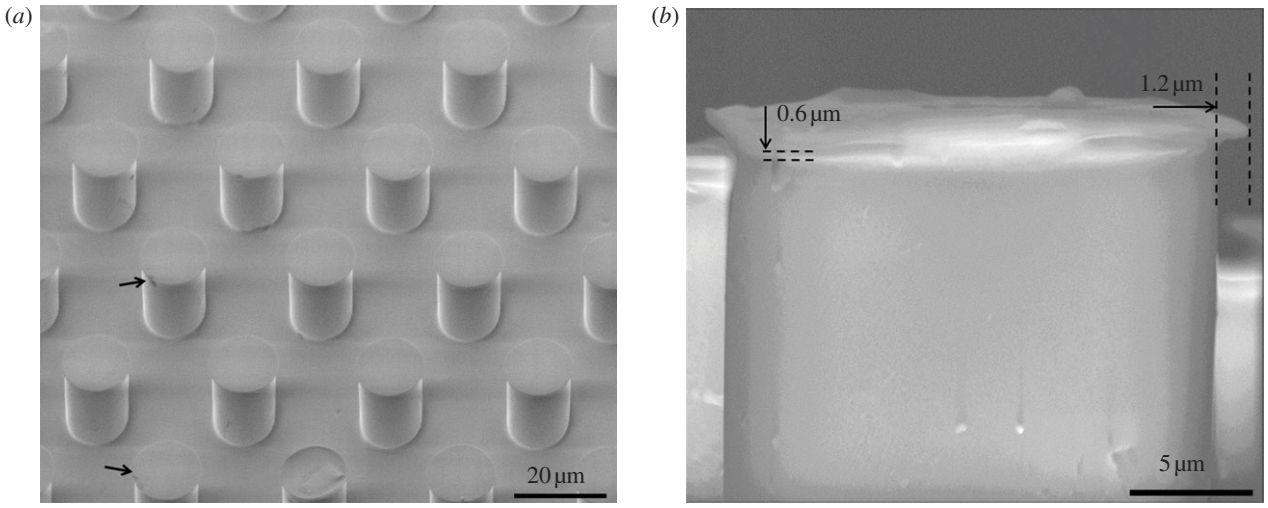

Figure 2. Type 1 fibrillar adhesive. Scanning electron micrographs of (*a*) aspect ratio (AR) 2 fibrillar arrays, and (*b*) a fibril with an end-flap. Arrows in (*a*) point to defects in end-flaps (less than 10% incidence within tested area). Dimensions of end-flaps are shown in (*b*).

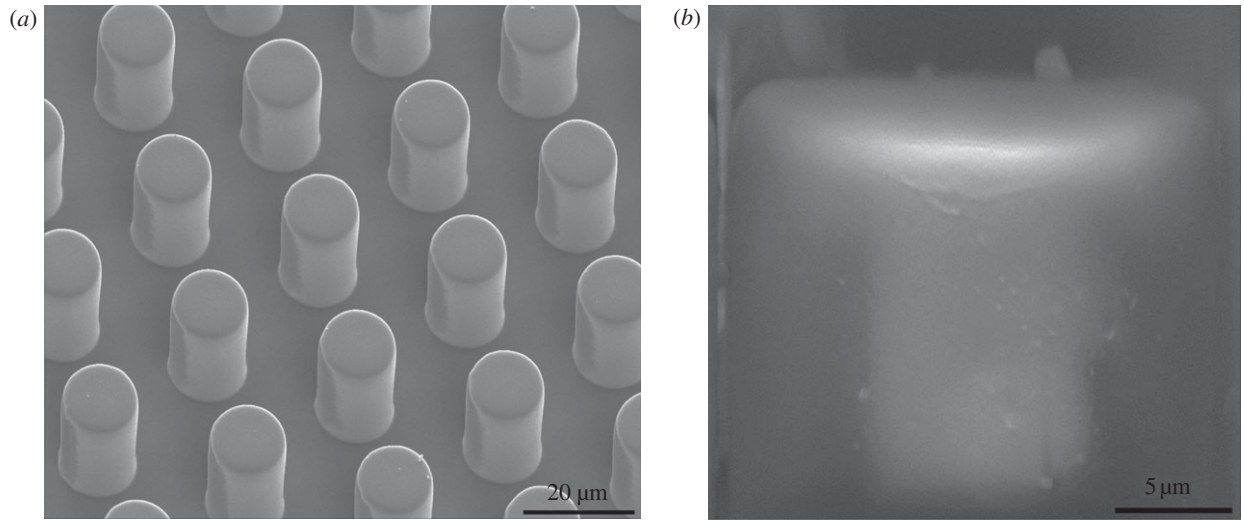

Figure 3. Type 2 fibrillar adhesive. Scanning electron micrographs (*a*) of AR 2 fibrillar arrays and (*b*) of a fibril with a round edge having a radius of approximately 0.85 µm.

gaps at the interface. Upon curing, when the PDMS was carefully peeled off the SU-8 master, it was patterned with fibrils with thin flaps at their ends. Uneven distribution of thermal stress led to variations in the delamination gaps. This, in turn, affected the shape and size of the resulting end-flaps. Some submicrometre-sized defects in the flap periphery or variations in its thickness were also observed (figure 2). The dimensions of the end-flaps were estimated using high-magnification scanning electron microscopy images. Flap width and thickness were measured at 2–3 different places and repeated thrice on one fibril to obtain the standard deviation.

The end-flaps are similar to the 'mushroom-shaped' structures published earlier [11,15], with the exception that the flaps here are generally much *smaller* relative to the fibril diameter.

2.2. Fabrication of micropillars having tips with round edges: type 2 fibrils

Finite deformation owing to surface tension effects has been observed in soft solids such as PDMS [16,17]. Given a sharp corner in the SU-8 master, a slight rounding of the fibril edge results in the PDMS replica owing to surface tension effects [16]. Through use of a second moulding step, such rounding effects on fibril edges can be amplified. The SU-8 master consisted of an array of cylindrical pillars. A primary mould of PDMS was replicated from the SU-8 master to generate an array of hexagonally packed holes. A second moulding step was carried out using the primary PDMS mould as the new master. Prior to pouring liquid PDMS on the primary PDMS mould, it was thoroughly silanized to avoid sticking (for details refer to Paretkar *et al*. [8]). After curing and demoulding, the resulting PDMS fibrils had round edges (figure 3). The edge radius of the fibrils was approximately 0.85 µm.

2.3. Adhesion testing

2.3.1. Test method

Adhesion tests were performed on a macroscopic adhesion testing device [18] and Microtack [19] using a flat test probe ($d = 1$ mm, polished steel cylinder). The flat probe was mounted on a double-beam spring of spring constant $k = 430\ \mathrm{N\ m^{-1}}$ and a rigid force sensor, respectively. The PDMS sample was attached on its non-structured side onto a glass slide using oxygen plasma activated bonding. The translucent PDMS adhesive sample allowed for visualization of the fibril–probe interface by optical microscopy. Videos of the images from such microscopy were recorded. The probe was first moved towards the sample until compression of it

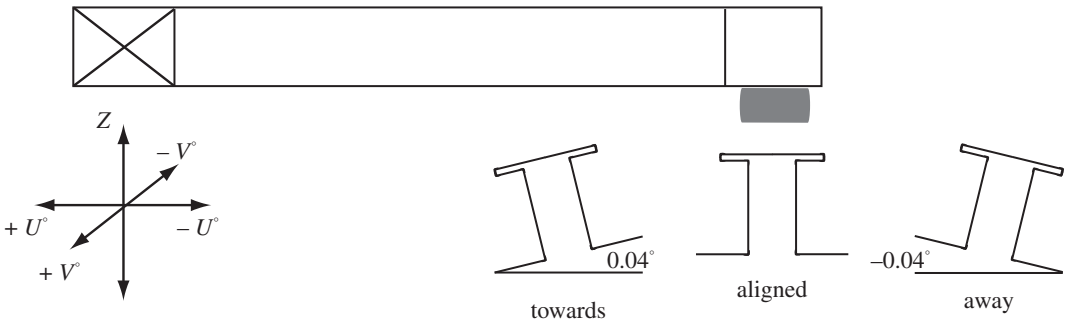

Figure 4. Schematic showing three fibril orientations rotated around the *V*-axis parallel to the probe/double-beam. The probe is a flat polished steel cylinder, $d = 1$ mm (grey not drawn to scale).

developed, and later the probe was retracted. The probe velocity on both approach and retraction was 10 µm s^{-1}. Different maximum preloads were achieved by controlling the degree of sample compression and the resulting pull-off forces were recorded. Preload stress is defined as the applied maximum compressive force divided by the test probe area (i.e. nominal contact area), and pull-off strength is defined as the measured maximum tensile force divided by the test probe area.

2.3.2. Sample alignment

Alignment of the fibrillar sample with respect to the flat test probe was closely controlled. The parallel sample–probe alignment was found by systematic changes of the sample orientation with respect to the probe/double-beam and comparison of the resultant pull-off forces at a predefined preload [8]. The aligned state yielded invariance of pull-off force for changes within 0.02° in both *U* and *V* orientations, both orthogonal to the approach axis, *Z* (figure 4).

To study the effect of tip shape on contact adaptability as a function of preload, the fibril alignment was systematically varied relative to the reference aligned state (figure 4). The sample was tilted in steps of 0.04°, in the positive and negative *U* directions (keeping the *V* tilt unchanged) and, therefore, in the aligned configuration. For each sample–probe alignment, an entire range of preloads were applied and corresponding pull-off forces were recorded.

3. Results

3.1. Aspect ratio

Figure 5 shows the measured pull-off strength as a function of preload stress for various ARs of type 1 (figure 5*a*) and type 2 (figure 5*b*) adhesives. Control samples of flat PDMS having similar thicknesses (2–2.5 mm) to those of the structured samples were also tested.

Flat PDMS controls had pull-off strengths of around 0.035 MPa that were insensitive to the preload stress. Repeated tests showed variations of less than 10 per cent in pull-off forces over the range of preloads investigated.

Type 1 adhesives exhibited higher pull-off strengths than flat controls. For a range of low preload stresses (0–0.1 MPa), pull-off strengths increased with applied stress for all samples with AR > 1. The increase in adhesion strength continued up to a preload stress of 0.03 MPa for the lowest AR of 1.4. For higher preload stress, the pull-off strengths of type 1 adhesives, with the exception of AR = 1, fell to levels even below those of flat PDMS. For example, the transition to a state of negligible adhesion was achieved around 0.2 MPa for AR 2.4, and around 0.45 MPa for

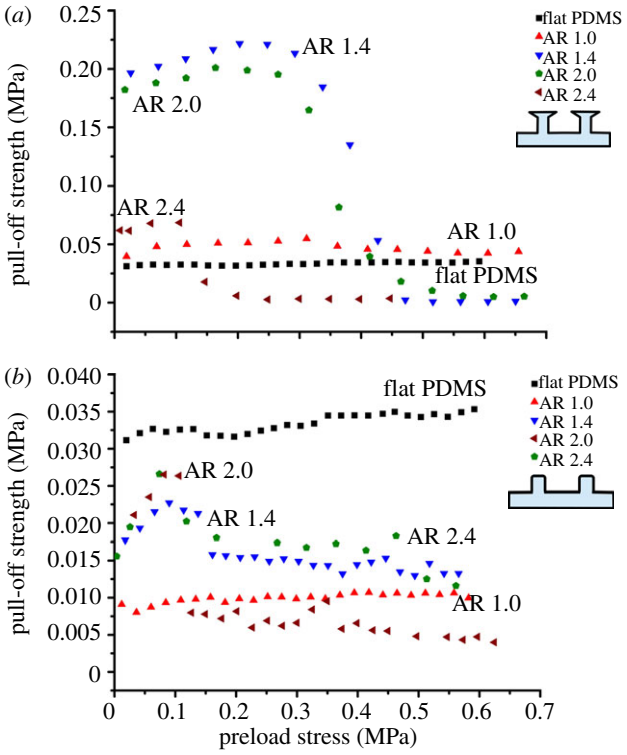

Figure 5. Pull-off strengths as a function of preload stresses for various AR adhesives of (*a*) end-flap terminated fibrils (type 1) and (*b*) round edge fibrils (type 2). ARs 1.4, 2 and 2.4 show a drop in adhesion at various preload stresses (experimental error within the size of the symbols). (Online version in colour.)

AR 1.4 and 2. Stresses at which a significant loss in adhesion was measured were recorded as adhesion loss stresses σ_{loss}.

Type 2 adhesives showed pull-off strengths typically 20–30% lower than those of flat control samples (figure 5*b*). AR 1 showed exceptionally low pull-off strengths. For a lower range of preload stresses (less than or equal to 0.1 MPa), pull-off strengths increased monotonically for all samples with AR > 1. The pull-off strengths fell rapidly with further increase in preload stress (greater than 0.1 MPa). Adhesion loss occurred at preload stress (σ_{loss}) > 0.17 MPa for AR 1.4, 2 and 2.4 of type 2 adhesives, such that the largest stress was required for the smallest AR.

3.2. Stress–time plots

When the preload reached a certain critical value, a *kink* in the stress was observed during the *loading* (figure 6). The corresponding stress was taken to be the *buckling stress* (σ_{crit}). For example, σ_{crit} was measured, from the inflection in stress (figure 7*a*,*b*), to be approximately 0.13 MPa for type 1 at 78.1 s and approximately 0.12 MPa for type 2 at 37 s for AR 2

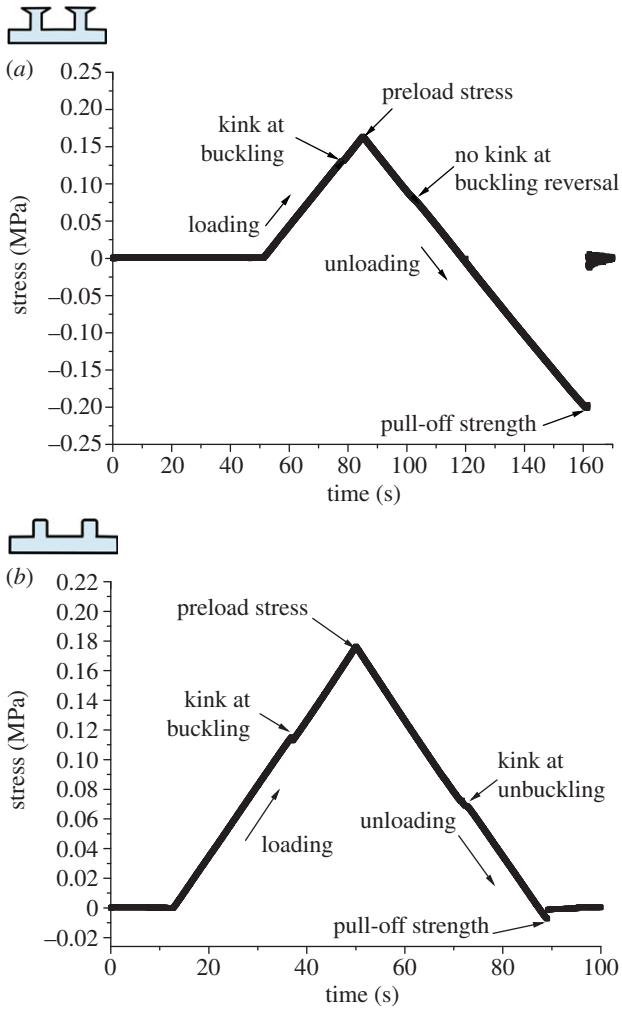

Figure 6. Evolution of stress in time during an adhesion test for AR 2 adhesives of (*a*) type 1 and (*b*) type 2. A compressive preload of 0.18 MPa, which is greater than the critical stress (σ_{crit}), is reached. Note kinks in stress at buckling and unbuckling (marked by arrows). Kink at buckling reversal (i.e. unbuckling) is absent for type 1. Positive stress indicates compression with a maximum corresponding to the 'preload stress'; negative stress indicates tension with a minimum denoting the 'pull-off strength'. (Online version in colour.)

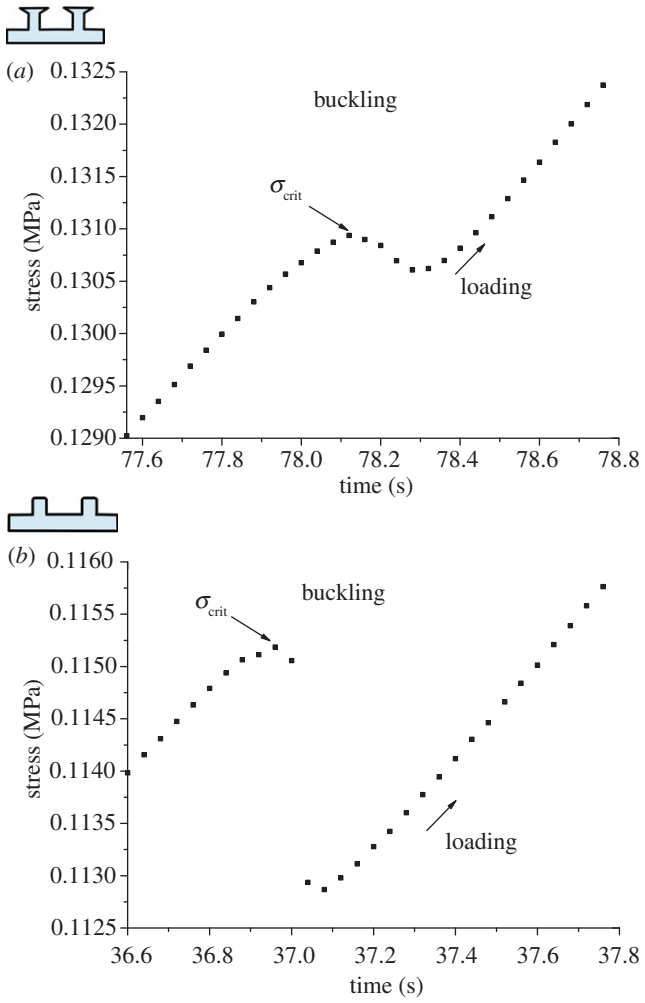

Figure 7. Critical stress (σ_{crit}) at buckling shown zoomed in from the loading parts of the curves in figure 6 for (*a*) type 1 and (*b*) type 2 adhesives. A smaller kink at buckling for type 1 is seen compared with that for type 2. (Online version in colour.)

adhesives during loading to a preload stress of 0.18 MPa (figure 7*a*,*b*). Type 1 adhesives exhibited a small stress change (0.3 kPa) and a gradual slope change during buckling compared with the change in type 2 adhesives (2.3 kPa; figure 7*a*,*b*).

The *unloading* from the preload stress of 0.18 MPa showed reversal of buckling (figure 8): whereas a gradual change in stress, without a kink, was characteristic for type 1 adhesives (figure 8*a*), type 2 adhesives exhibited a step-like change in stress during buckling reversal (figure 8*b*). Furthermore, it was observed that for *unloading* from a high preload stress of 0.5 MPa, larger kinks appeared during buckling reversal for both adhesive types (figure 8*c*,*d*). Table 2 summarizes the measured critical stresses (σ_{crit}) as well as the adhesion loss stresses (σ_{loss}) for both types of adhesives.

3.3. Video results

Buckling and unbuckling were observed during the adhesion tests with the help of an optical microscope. For type 1 adhesives, during loading, a transition from top to side contact was observed concurrent to buckling (figure 9*c*). During unloading, upon unbuckling, the fibril tips re-formed contact (figure 9*d*). Immediately after this transition, series of localized bright spots appeared and disappeared over a period of around 10 s (figure 9*e*), and were taken as indicators of the end-flaps themselves unfolding. Subsequently, unloading proceeded into tension, and a detachment front was observed to proceed from the top edge of the circular contact with progressive release of fibrils (arrows in figure 9*f*). Type 2 fibrils do not exhibit any bright spots after the buckling reversal (see the electronic supplementary material, figure S1).

3.4. End-flap orientation

Figure 10 shows the effect of sample alignment on adhesion for type 1 adhesives having AR 2. Loss of adhesion strength at high preload was not observed when the sample was tilted *'away'* by 0.04° relative to the probe/double-beam, whereas there is significant adhesion loss at high preload in the '*aligned*' state (figure 10*a*,*b*); this result was reproducible at different locations on the sample (see the electronic supplementary material, figure S5). Type 2 adhesives failed to show any drastic changes in adhesion strength as a function of sample alignment (see the electronic supplementary material, figure S6).

4. Discussion

The central observation of this paper is the instability of the pillars under compressive preloading as evidenced by the kinks in the force–time plots. These instabilities were attributed to elastic

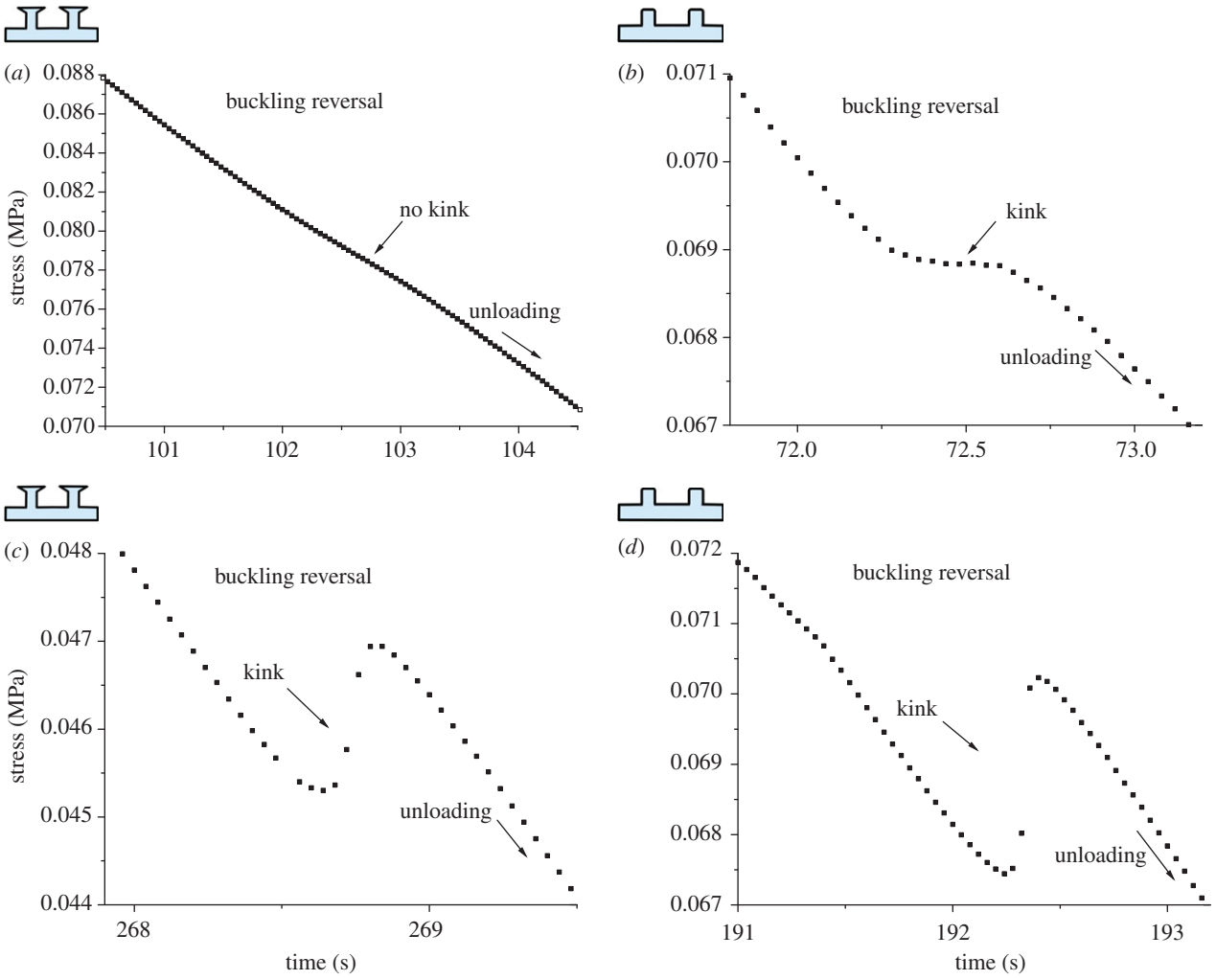

Figure 8. Critical stress at buckling reversal (or unbuckling) shown zoomed in from the unloading parts of the curves in figure 6 for (*a*) type 1 and (*b*) type 2 adhesives. No kink is seen for type 1 adhesives, whereas a step-like change in stress is observed for type 2 adhesives during reversal of buckling from a preload of 0.18 MPa. In comparison, buckling reversal from a high preload stress of 0.5 MPa is dominated by large kinks in stress for (*c*) type 1 and (*d*) type 2 adhesives. (Online version in colour.)

Table 2. Observed critical buckling stresses (σ_{crit}) and adhesion loss stresses (σ_{loss}) for type 1 and type 2 adhesives.

	type 1			type 2		
AR	σ_{crit} (MPa)	σ_{loss} (MPa)	pull-off strength maxima (MPa)	σ_{crit} (MPa)	σ_{loss} (MPa)	pull-off strength maxima (MPa)
1.4	0.21 $\pm$ 0.002	0.47	0.22	0.15 $\pm$ 0.006	0.16	0.022
2	0.13 $\pm$ 0.003	0.56	0.20	0.11 $\pm$ 0.003	0.13	0.026
2.4	0.11 $\pm$ 0.001	0.25	0.06	0.10 $\pm$ 0.01	0.10	0.027

buckling and were, for higher preloads, accompanied by a drop in adhesion strength. As expected for Euler–Bernoulli buckling, the drops in pull-off strengths (adhesion) occurred at lower preload stresses for samples with higher AR pillars. However, there are important distinctions between the two types (1 and 2) of adhesives with respect to the following.

(1) The stress at which buckling occurred (σ_I) for different ARs.
(2) The stress at which adhesion loss (σ_{loss}) occurred at constant AR (table 2).
(3) Pull-off strength maxima as a function of ARs (figure 5).
(4) Dependence of adhesion loss stress (σ_{loss}) on sample alignment (figure 11).

The discussion aims to address these four points.

4.1. Point 1: fibril buckling and unbuckling

The critical buckling condition owing to Euler–Bernoulli theory is given by the following equation [20]:

$$F_{crit} = \frac{n^2\pi^2 EI}{h^2}, \tag{4.1}$$

which can be expressed for a circular cross section as

$$\sigma_{crit} = \left(\frac{n^2\pi^2 E}{128\sqrt{3}}\right)\frac{1}{(h/d)^2}, \tag{4.2}$$

where F_{crit} and σ_{crit} are the critical load and stress, E is the Young's modulus of the fibril (assumed as 3.4 MPa for the PDMS material), I is the second moment of area, where $I = (\pi d^4/64)$ for a circular cross section with diameter d and

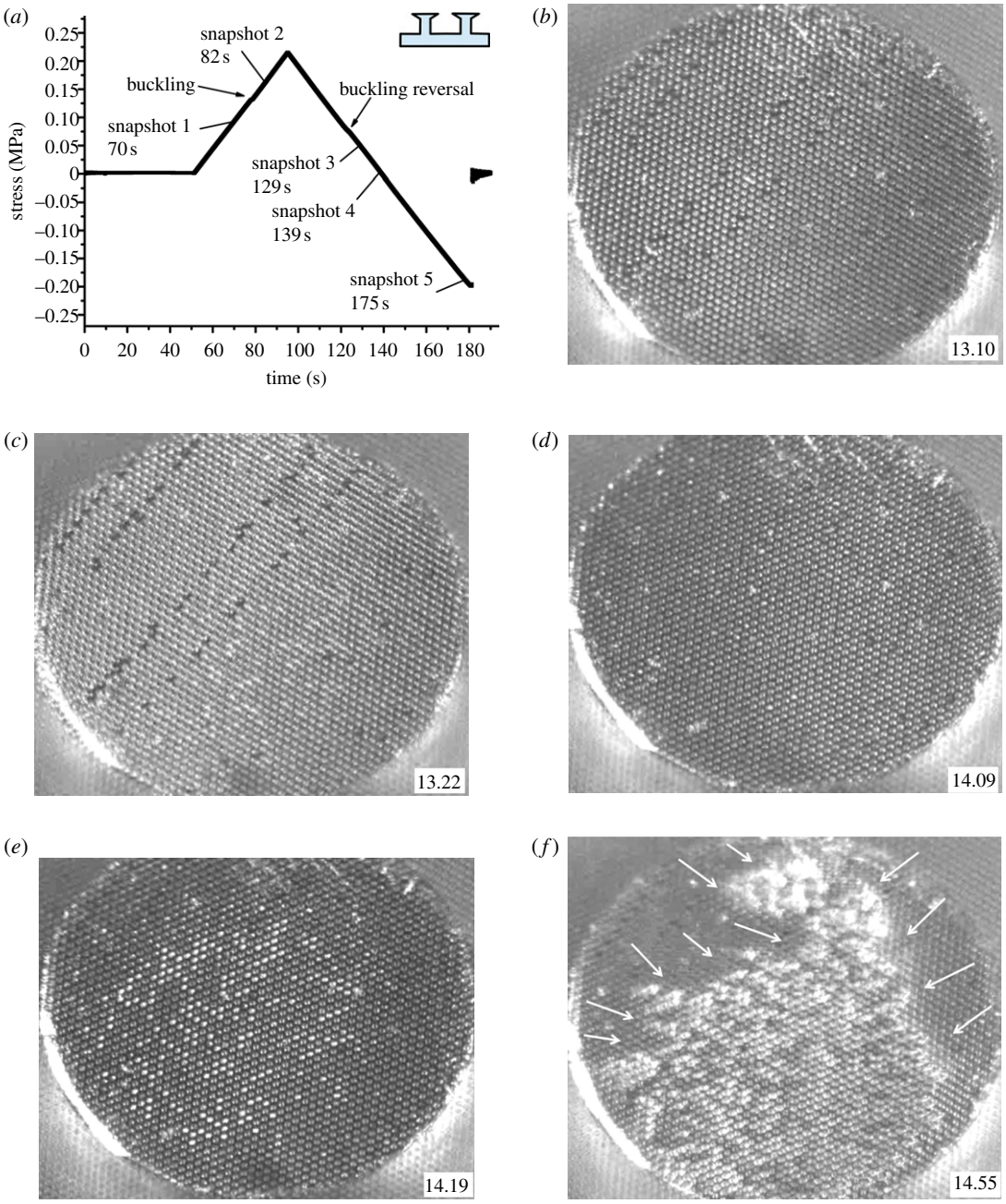

Figure 9. Buckling transition for type 1 AR 2 adhesives. (*a*) Stress–time plot with marked points corresponding to video snapshots at given times: (*b*) snapshot 1, fibril tips in full contact; (*c*) snapshot 2, fibrils in side contact after buckling; (*d*) snapshot 3, fibril tips back in contact upon buckling reversal; (*e*) snapshot 4, localized bright spots near centre; and (*f*) snapshot 5, partial detachment before pull-off with arrows marking detachment front (black spots are defects on the probe surface and are considered irrelevant). (Online version in colour.)

length h, and AR $= h/d$ is the AR of the pillar. The pre-factor n is related to the half-wavelength of the buckled shape and takes different values depending on the end constraints on the fibril. The hexagonal packing of the fibrils (area fraction of 22.67%) was accounted for by modifying equation (4.1) in order to estimate the theoretical stress per pillar.

Figure 11 shows the comparison of the experimental critical stress (points) with those predicted by the Euler–Bernoulli buckling theory (straight lines) for the two adhesive types. The different lines represent the theoretical buckling stresses for different end constraints (i.e. pre-factor, n) on the fibrils. In our case, one end of the fibril is always clamped by the backing, whereas the other end may be: (i) free to translate or rotate ($n = 0.5$), or (ii) free to translate but not rotate ($n = 1$), or (iii) free to rotate but not translate ($n = 1.43$). Figure 11 shows that all but one data points come to lie between the cases $n = 1$ and $n = 1.43$; this behaviour probably reflects the nature of the probe (spring-like, stiff, etc.), and the adhesion between the fibril and the probe.

The slope of the load–displacement curve helps estimate the total stiffness of the fibrils and the backing [21]. The results appear to follow the Euler buckling theory: higher AR fibrils buckled at lower stress. Measured σ_{crit} for all ARs appear to be slightly higher than the theoretical stress for the end constraint of $n = 1$. This may be rationalized as follows: prior to buckling, the fibrils are constrained at both ends, at one by the backing and at the other by the adhesion with the probe. Forces applied need to overcome the fibril–probe adhesion before top contact is lost upon buckling, leading to $n > 1$. This result is consistent with the theoretical study of Stark *et al*. [22]. It is noted that the Euler–Bernoulli buckling theory applies to long, slender

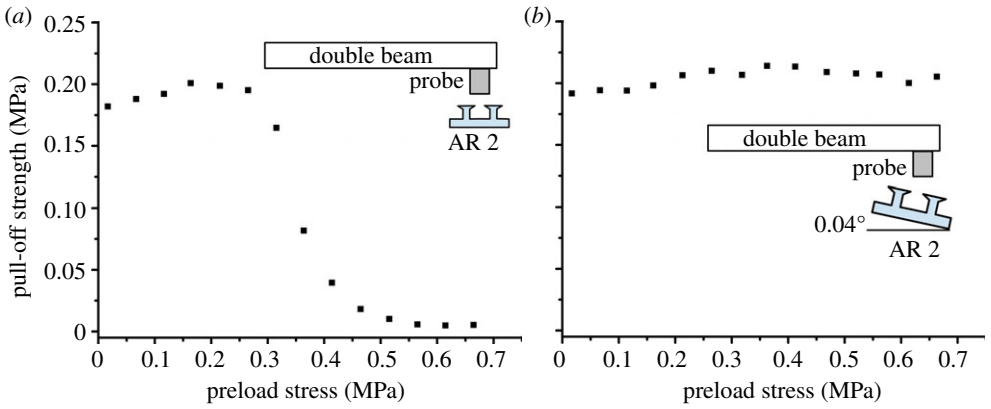

Figure 10. Sample alignment effects on adhesion in type 1 adhesives. (*a*) Adhesion loss and (*b*) no adhesion loss for the same set of preload stresses for AR 2 type 1 adhesives. Inset: schematic of the sample in (*a*) 'aligned' state and (*b*) tilted 'away' by 0.04° with respect to probe–double-beam. (Online version in colour.)

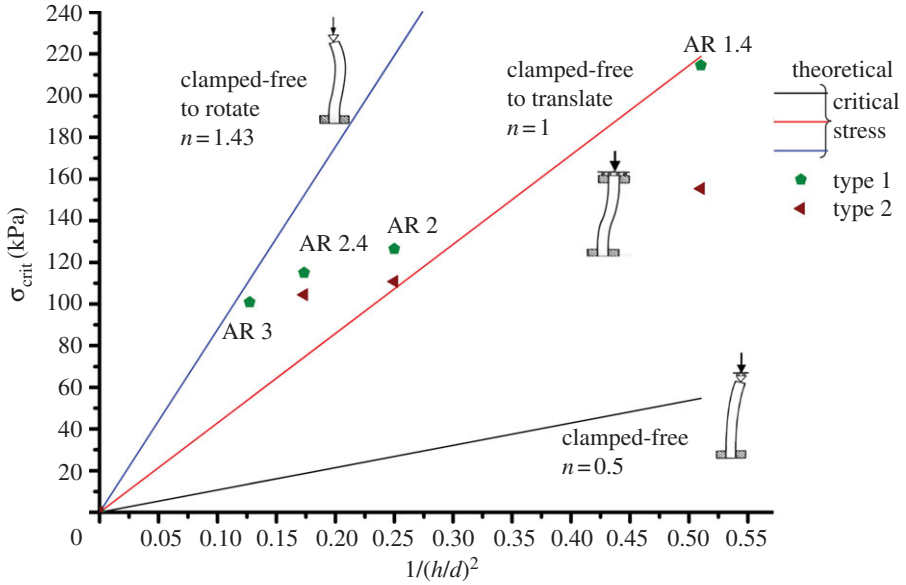

Figure 11. Theoretical Euler–Bernoulli buckling stress (lines) and measured critical stress (points) per pillar for type 1 and type 2 adhesives plotted as a function of $1/(AR)^2$ following equation (4.2). The slopes of the lines reflect the different end constraints on the fibril, schematically depicted in the thumbnail sketches. For type 1 adhesive an extra point corresponding to measured critical stress for AR 3 is included as investigated in [8]. (Online version in colour.)

fibrils ($h \gg d$, AR > 7) in the absence of shear forces. In view of the relatively low AR of our fibrils and the spring-like flat probe surface, both of these conditions are not strictly met. Nevertheless, the agreement is encouraging.

Given that all the fibrils unbuckle completely before the interface is subjected to tension, a valid question arises. If the fibrils return to their original state before being pulled off from the substrate, why does the buckling event have any effect on the pull-off strength? One possible reason could be that a certain duration of time is required after contact to regain adhesion. However, we rule out this hypothesis as the adhesion experiments are carried out sufficiently slowly. A second reason could be that the interface only apparently returns to its original state. This hypothesis is schematically depicted in figure 12 along with corresponding high-magnification pictures from the *in situ* adhesion test.

State (1) depicts a single fibril prior to buckling; state (2) represents the same fibril just after buckling. Note that a shear force is required to keep the fibril from losing top contact after it has buckled. If the contact area is small, and generally this is the case, and if friction is insufficient to support the required shear load, the fibril will slide into side contact, as shown in (3). On *unbuckling* (4), the top of the micropillar is stuck at a distance s from the upright position where it originally made contact with the probe in an unstressed state. Corresponding high-magnification pictures show these events ending in an unbuckled fibril with a remnant slip.

Suppose that the fibril has a slip of distance s after unbuckling. It has now formed full contact at the end and let us assume that there is sufficient friction so that the fibril does not slip back. We now subject the fibril to tension. Because of the slip, we will get additional shear and a bending moment at the contact. These will change the stress distribution on the contact. Imagine that the force to separate the fibril from the probe is governed by growth of some flaw at the edge of the fibril.

By calculating the energy release rate (or stress-intensity factors) at the putative flaw, we can examine how slip affects the pull-off process [23]. The stress-intensity factor, assuming that mode I dominates, is a sum of two contributions:

$$K_F + K_m = \sqrt{E \times W_{ad}}, \tag{4.3}$$

where K_F is the stress-intensity factor owing to normal load F and K_m is the stress-intensity factor owing to the bending moment.

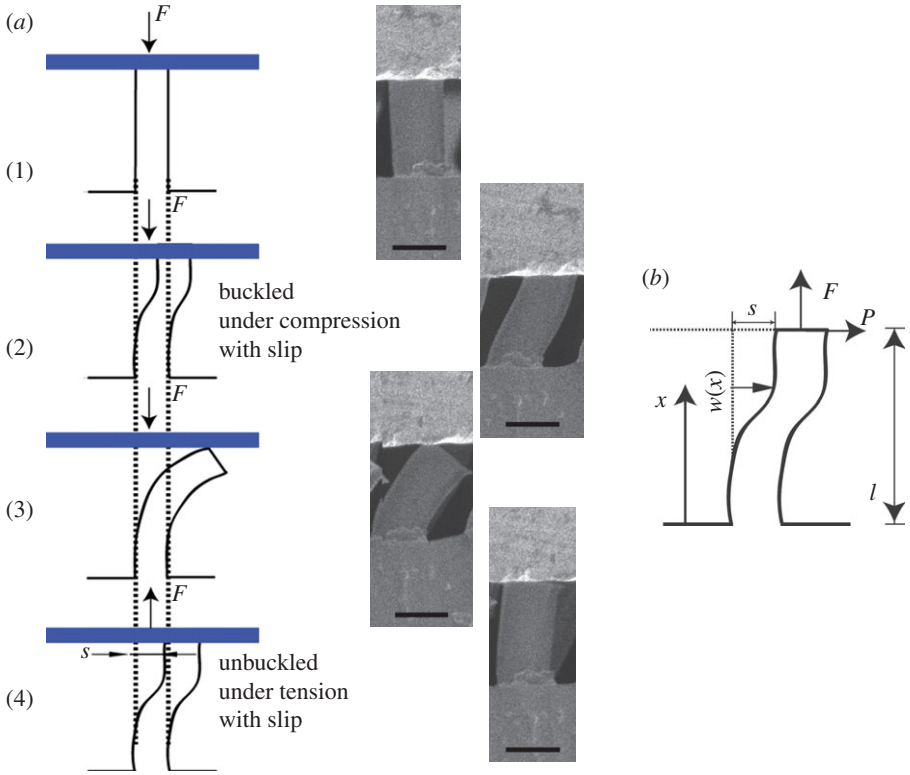

Figure 12. (*a*) Sequence of fibril configurations (1) prior to buckling, (2) buckled with shear, (3) contact loss and (4) unbuckled with a remnant slip. Corresponding *in situ* scanning electron microscopy images from an adhesion test showing fibril states (centre). Scale bar, 10 µm. (*b*) Force distribution on the fibril after the unbuckling with a slip *s* and shear *P*. (Online version in colour.)

For a small crack of length *c* and a fibril with diameter *a*, these are given by [24] (see the electronic supplementary material for detailed derivation)

$$K_{\mathrm{tot}} = K_{\mathrm{F}} + K_{\mathrm{m}} = 1.12\frac{F}{a^2}\sqrt{\frac{c}{\pi}}\left[0.5 + \frac{4s}{a}\frac{\sinh(\sqrt{F}/2)}{\sqrt{F}\cosh(\sqrt{F}/2) - 2\sinh(\sqrt{F}/2)}\right]. \tag{4.4}$$

Clearly if we equate the left-hand side of equation (4.4) to a material property, we have a transcendental equation in force. However, to make the point about the importance of slip *s*, it is sufficient to examine the term $\sinh(\sqrt{F}/2)/(\sqrt{F}\cosh(\sqrt{F}/2) - 2\sinh(\sqrt{F}/2))$. Based on our experimental parameters the term above is then of the order of 16. For example, a fibril with AR 2 with pull-off strength of 0.2 MPa would, without a slip of say 2 µm, show a pull-off strength 25 times higher, i.e. about 5 MPa using the above calculations (see the electronic supplementary material, table S1, for different *s*/*a* ratios). This shows that a slip of even a fraction of the fibril radius will reduce pull-off load significantly. Thus, the mean strength of the fibril–probe interface reduces as each micropillar returns back into top contact after unbuckling with a variable *s* and the overall reduction in the strength will depend on the statistical variation.

4.2. Point 2: stresses for adhesion loss

Figure 13 compares the buckling stresses (σ_{crit}), as identified from the kink in the force–time plots, and the adhesion loss stress (σ_{loss}) for the two types with AR 2. It is clear that, for type 1 adhesives, a buckling transition need not necessarily result in an adhesion loss as was previously reported [24,25]. Type 2 adhesives, in contrast, do not show a significant difference between σ_{crit} and σ_{loss}.

This discrepancy is discussed here exploring the nature of fibril contact transition upon buckling reversal.

4.2.1. Preload regime 1

Stress regime 1 is defined by the preload stress between 0.13 and 0.28 MPa (figure 13). In this regime, type 1 adhesives retained high pull-off strength, whereas adhesion dropped drastically for type 2. It is postulated on the basis of *in situ* video results that, after the fibril contact transition, the end-flap (of type 1 adhesives) folded on itself, adopting either of the two configurations illustrated in figure 14. It must be noted that owing to the variation in the end-flap geometry the folding/unfolding of the end-flap may not be the same for all fibrils.

Increasing compressive stress almost always enforced the folded end-flap configuration, i.e. configuration 2 shown in figure 14*b* (confirmed by *in situ* video analyses, figure 9). The folded end-flap thus maintained a link between the fibril top and the probe. Such a link is proposed to be crucial for re-establishing a smooth contact during unloading. After the reversal of fibril buckling the end-flap unfolds assisting the fibril contact re-formation. Type 1 adhesives, owing to the smooth sealing facilitated by the end-flaps, show a relatively smaller kink (or even absence of it altogether) compared with type 2 (figure 8*a*).

The folding of end-flaps under compression was previously observed by Varenberg & Gorb [26] for similar tip shapes. In their case, the end-flaps were in the form of a more pronounced mushroom-like shape than the present case. The folding–unfolding behaviour of the end-flaps, together with their superior contact adaptability [27,28], may explain the high adhesion in spite of the reversible buckling.

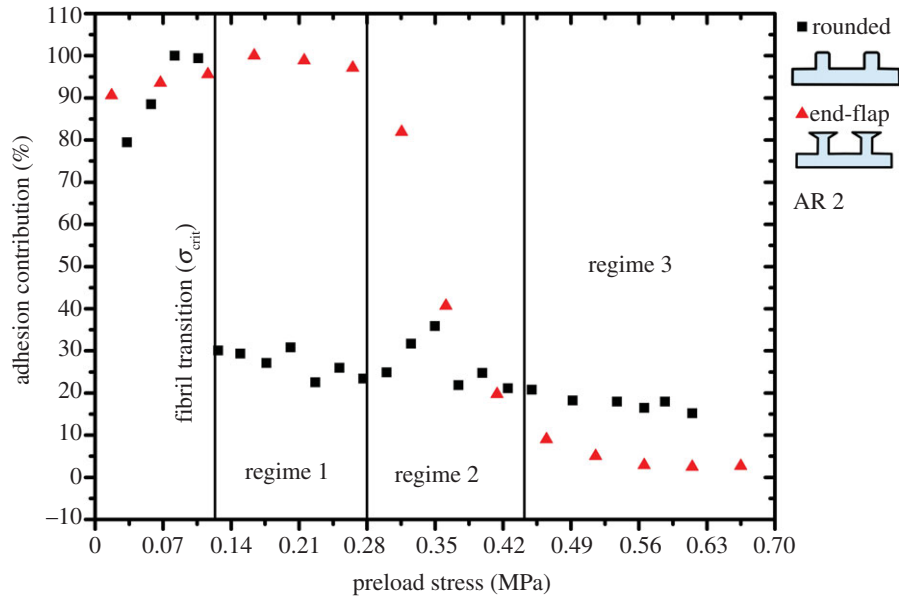

Figure 13. Adhesion contribution (percent of the maximum adhesion strength) as a function of preload stress for both adhesive types. Stresses slightly greater than critical are defined by regime 1, intermediate stresses by regime 2 and very high preload stresses by regime 3. Adhesion loss for type 1 occurred at much higher stress compared with type 2, which showed loss concurrent to critical stress. (Online version in colour.)

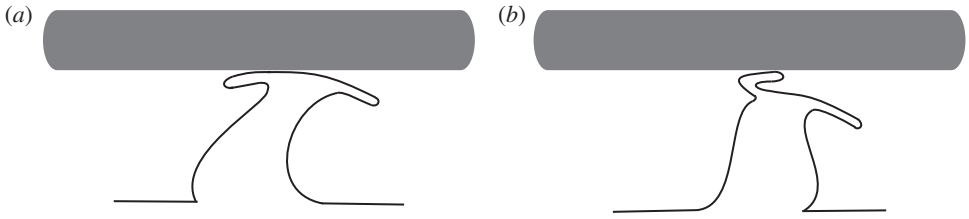

Figure 14. Schematic based on video data showing two possible configurations for end-flap folding during the fibril contact transition at preloading: (*a*) configuration 1 and (*b*) configuration 2. Configuration 2 appeared more probable for stresses in regime 1 as the videos of the unloading contact transition showed optical changes in brightness just after the fibrils regained vertical shape (figure 9).

In contrast, type 2 fibrils with round edges lost the top contact entirely during buckling. When the buckling reversed during unloading, the round edges acted as circumferential defects that hindered smooth sealing of the interface during the fibril contact re-formation. This led to the observed larger kinks in stress at unbuckling during unloading (figure 8*b*). Hence, type 2 adhesives showed adhesion loss for all preload stresses above the buckling stress (σ_{crit}).

4.2.2. Preload regime 3

Stress regime 3 is defined by *very high preload stress* (greater than or equal to 0.45 MPa; figure 13). In this regime type 1 adhesives having AR 2 also showed negligible adhesion.

A systematic lowering of the stress at which unbuckling occurs was noted as a function of the preload stress for type 1 adhesives (figure 15*a*). This in turn meant that during the unloading process the unfolding of the end-flap, which immediately follows the unbuckling, had continually lower compressive stresses available for contact re-formation at higher applied stresses.

The unbuckling event at the high preloads shows a characteristic large kink in stress. Such a kink was indicative of an abrupt fibril contact transition from the prone to the vertical state. Once vertical, the lack of sufficient compressive stress hindered the unfolded end-flap's ability to form an intimate contact with the probe. The resultant drastic loss in contact area was responsible for the adhesion loss.

For type 2 adhesives, in contrast, stress at which buckling reversal took place did not vary much (figure 15*b*).

4.2.3. Video analysis: preload regimes 1 and 3

We consider two cases for an adhesive sample of type 1 where applied load belonged to preload regime 1 in one case and to preload regime 3 in the other. MATLAB was used to analyse the changes in the average light intensity at the contact interface that occurred during the detachment process. Figure 16 shows the changes in the average intensity at the interface from the point in time when all the fibrils have unbuckled (i.e. appear to be vertical) to the point when they have all detached. An overall increase in the average intensity of light at the interface was observed during detachment. More light is able to reach the interface from the source of illumination below the sample once the fibrils are in tension and/or get peeled off the probe at an angle away from the vertical. On the other hand, less light reaches the interface when all fibrils are vertical and in intimate contact with the probe.

For applied preload in regime 1 unbuckling of fibrils took place within the first 2 s (frames 0–50; figure 16*a*). This was followed by a slight rise and a small dip in the average intensity for the appearance and disappearance of localized bright spots (frames 50–400 or over 10 s; figure 9, snapshot 4). Greater amount of light reached the interface prior to the unfolding of the flaps when the fibril tip is at an angle to the probe. A slight dip in the average intensity was seen as

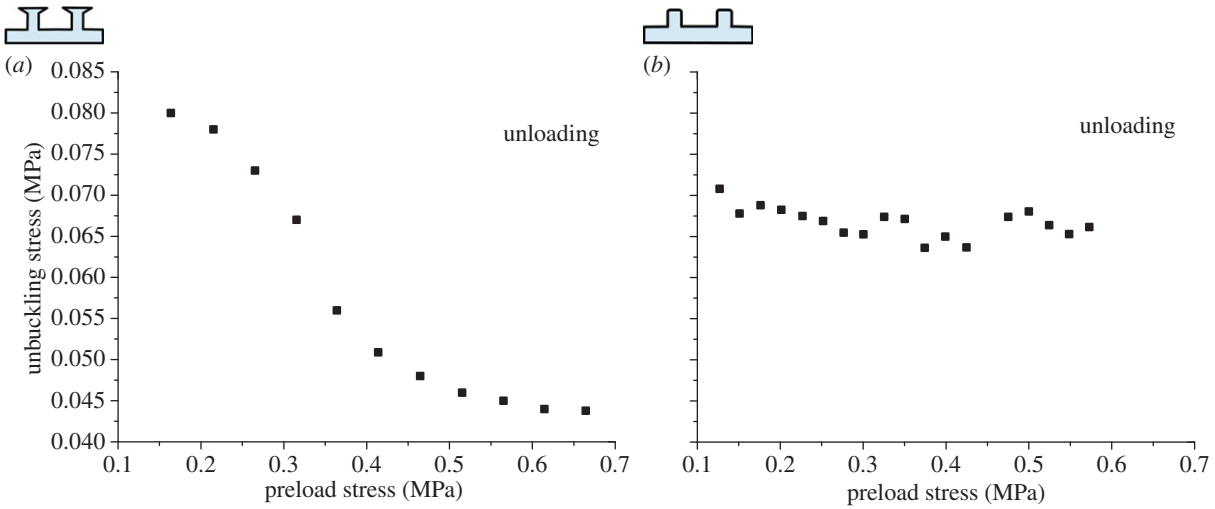

Figure 15. Stress at unbuckling. (*a*) Type 1 adhesives undergo unbuckling at continually lower stress compared with almost constant stress for buckling reversal in (*b*) type 2 adhesives for the same range of preload stress. Type 1 adhesives, therefore, have lower compressive stress available prior to detachment at high preload stresses (greater than 0.45 MPa). (Online version in colour.)

the flap unfolded making full top contact and thereby blocking light. A steady increase in the average intensity was further observed for progressive detachment of fibrils over approximately 900 frames or 30 s (frames 400–1300), with a sharp dip at the end when all the fibrils are vertical again and have lost the contact with the probe.

In figure 16*b*, on the other hand, the detachment occurred very rapidly within 200 frames or within 7 s (frames 50–250). The short increase in intensity was owing to the fibrils orientating away from the vertical prior to peeling rapidly off flat probe followed by a sudden drop when the fibrils lost contact with the probe (see the electronic supplementary material, figure S2, snapshot S4).

The type 1 fibrils appear to detach progressively from the probe in the case of reduced adhesion after buckling transition (preload regime 1, figure 9, snapshot 5) as opposed to a sudden release in the case of no adhesion after buckling transition (preload regime 3, electronic supplementary material, figure S2, snapshot S4). The former is an indicator of reduction in strength of the ensemble of fibrils owing to statistical reasons while the latter, a singular event of detachment, indicates a uniform reduction of fibril–probe strength.

As the preload increases from regime 1 to regime 3 through the intermediate regime 2 the statistical influence on the reduction of adhesion strength becomes less dominant whereas the uniform reduction in the interface strength appears to dominate.

4.2.4. Preload regime 2

Stress regime 2 is defined by an intermediate preload stress between regime 1 and 3 (for preload stress between 0.3 and 0.45 MPa, figure 13). In this regime, adhesion for type 1 adhesives falls from high to low values, whereas type 2 adhesives show low adhesion. For type 1, unbuckling during unloading occurred at continually lower stresses with the increase in preload stress (figure 16*a*). When the preload stress was low (approx. 0.3 MPa), the end-flap unfolding enabled contact re-formation and led to observed adhesion. This was attributed to the available compressive stress prior to detachment aiding the contact re-establishment with the probe. The events of buckling reversal, unfolding of the end-flap and detachment from the probe surface ensue, in the above order, very rapidly with no time and/or compressive stress available to re-form intimate contact with the probe.

Thus, adhesion of type 1 samples tends to be a function of the unfolding and contact re-formation, which by nature is stochastic and dictated by the preload stress within regime 2.

4.3. Point 3: adhesion strengths and aspect ratio

Generally, it is expected that higher AR fibrils, owing to their increased compliance, show higher pull-off strength [29,30]. However, the maxima in the pull-off strengths recorded for different ARs of type 1 adhesives did not follow this trend. This is attributed to minor variations in the shapes and sizes of the end-flaps owing to the process variability. The differences in the dimensions of the end-flaps for different ARs (table 1) can strongly affect adhesion and appear to dominate adhesion effects more than the compliance changes by AR variation [11,26]. Type 2 adhesives follow the general trend of higher adhesion for high AR samples. The pull-off strength depends on the distribution of stress and stress-intensity factors that are in turn governed by the geometry of the end-contact for fibrils with end-flaps [27].

The pull-off strength decreases sigmoidally with the preload stress beyond the critical preload. The slope at the centre of the sigmoidal transition increases with increasing AR of the adhesive.

4.4. Point 4: sample alignment

Tilting of type 1 fibrils *away* from the probe effectively orients the end-flaps, such that the contact of the top face may be retained over the entire loading–unloading cycle (figure 14, configuration 1). Thus, by changing the sample alignment, both low and high adhesion states can be obtained for the same high preload stress. Different sample alignments for type 2 adhesives with round edges failed to show a drastic adhesion response as a function of preload stress (see the electronic supplementary material, figure S6). The maxima in pull-off strength were lower in the 'misaligned' state, consistent with previous results [31].

The adhesives developed during this work demonstrated use in simple applications that need pick-and-place of an object. In designing pick-and-place robot systems, it is important that the mechanical instability of the fibrils is recognized

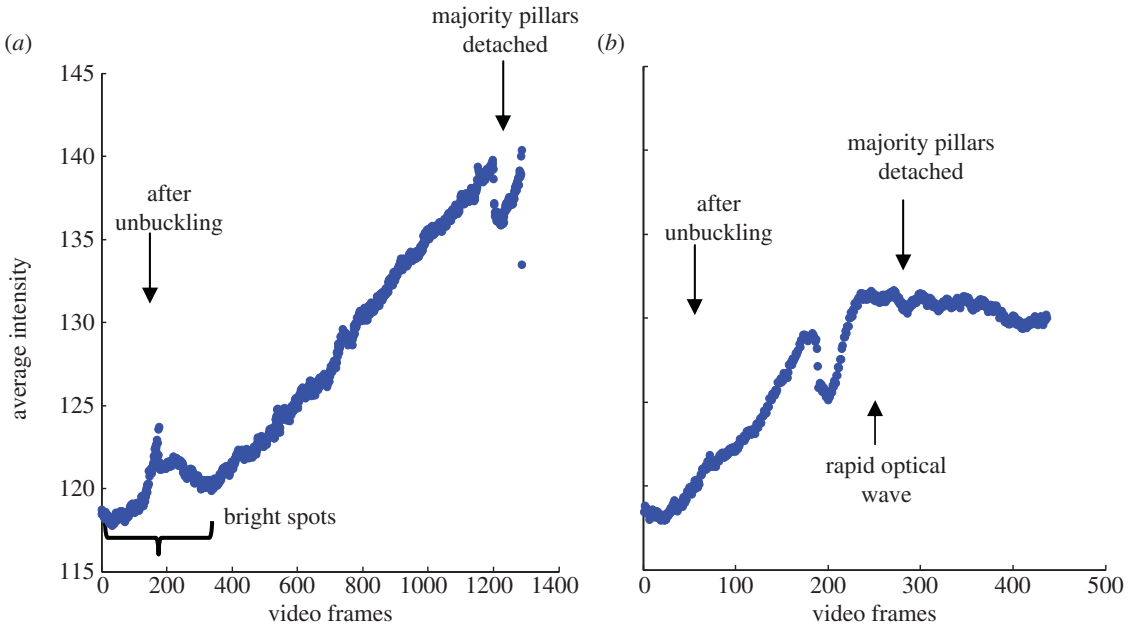

Figure 16. Video analysis of the detachment process after type 1 fibrils unbuckle for two different preload regimes. (*a*) For the applied preload in regime 1, after unbuckling (frames 0–50, or within 2 s) appearance and disappearance of bright spots owing to flap unfolding causes a slight dip in rising intensity (frames 50–400). The fibrils detach over 900 frames or a longer time (i.e. in 30 s). Higher average intensity is reached as more light reaches the interface when fibrils are pulled in tension and peeled off progressively at an angle different from vertical. (*b*) For the applied preload in regime 2, after unbuckling the detachment occurs within 200 frames or in a short time (i.e. within 7 s). Lower rise in average intensity occurred as the fibrils peel rapidly off the interface with a sharp dip at the end when the majority of fibrils lose contact. (Online version in colour.)

with respect to the applied load and orientation. The range of loads as well as the orientation at which fibrils hold the load (normal, shear or mixed) should be known to avoid accidental over-compression and loss of an object. End-flap terminated fibrillar adhesives have functioned even when they were not well aligned to the smooth surfaces. The invariance to alignment, combined with the possibility of achieving reversible, and repeatable adhesion render their use as switchable adhesives practical.

Their capability to lift a smooth glass plate (with/without weights) and its easy release by use of pressure or orientation change has been achieved. The lifting of a 500 g weight using a small strip of adhesive (contact area $\approx 1\ \mathrm{cm}^2$) is seen in the video (see the electronic supplementary material, video file). The strip was brought in contact with a glass plate to which a 500 g weight was attached. When both the adhesive and the area of contact on glass are clean, then no external pressure was required to form an adhesive contact. It was possible to lift the glass in normal as well as shear mode (shear stress less than or equal 0.5 MPa).

5. Conclusions

Preload-responsive adhesion was achieved in fibrillar surfaces by inducing buckling, and loss of contact between fibril tips and a stiff probe surface. The mechanism of adhesion transition was investigated by studying the effects of AR, tip shape and orientation with respect to the probe surface. The following conclusions can be drawn.

— Adhesives with higher AR fibrils showed adhesion loss at lower preload stress. Buckling of fibrils was observed *in situ* at preload stresses following the predictions of the Euler–Bernoulli buckling theory.
— Buckling was recognized to be reversible and it was found that the stress for adhesion loss (σ_{loss}) was not necessarily identical to the buckling stress (σ_{crit}). This was attributed to a re-configuration of the end-flaps in type 1 adhesives.
— Round tips in type 2 adhesives acted as a circumferential defect which impaired contact re-formation upon buckling reversal of the fibrils. Hence, buckling in these fibrils always resulted in adhesion loss.
— Fibrils with end-flaps (type 1) exhibited contact recovery by folding and unfolding during a reversible buckling event. In addition, at moderate preload sufficient compressive stress was available after buckling reversal to aid the contact re-formation. This led to reversible adhesion, which gradually diminished with increasing preload stress.
— Very high preload stress caused adhesion loss even in fibrils with end-flaps (type 1). Unbuckling events were associated with large kinks in stress at these preload stresses, indicative of an abrupt fibril contact transition. In addition, the end-flaps unfolded under insufficient compressive stresses after the buckling reversal. Hence, intimate tip contact re-formation was impaired and the resultant drastic loss in contact area was responsible for the adhesion loss.
— Systematic changes in fibril orientation with respect to the probe affected adhesion switching only for fibrils with end-flaps (type 1). This was explained on the basis of the orientation dependent folding–unfolding of the end-flap.
— The results of this study provide a mechanistic basis for designing new adhesives which can be switched from an adhesive to a non-adhesive state and back. Such surfaces can be useful in novel gripping and placement systems.

D.P. thanks Joachim Blau for the visualization appendage to the adhesion test device, and Elmar Kroner and Andreas Schneider for insightful discussions. This work, as a part of the European Science Foundation EUROCORES programme FANAS, was supported by the German Science Foundation (DFG) grant no. AR201/9-1. M.K. was supported by the Netherlands Organization for Scientific Research (NWO, VENI-700.10.404).

References

1. Kamperman M, Kroner E, del Campo A, McMeeking RM, Arzt E. 2010 Functional adhesive surfaces with 'gecko' effect: the concept of contact splitting. *Adv. Eng. Mater.* **12**, 335–348. (doi:10.1002/adem.201000104)
2. Jagota A, Hui CY. 2011 Adhesion, friction, and compliance of bio-mimetic and bio-inspired structured interfaces. *Mater. Sci. Eng. R* **72**, 253–292. (doi:10.1016/j.mser.2011.08.001)
3. Kamperman M, Synytska A. 2012 Switchable adhesion by chemical functionality and topography. *J. Mater. Chem.* **22**, 19 390–19 401. (doi:10.1039/C2jm31747h)
4. Reddy S, Arzt E, del Campo A. 2007 Bioinspired surfaces with switchable adhesion. *Adv. Mater.* **19**, 3833–3837. (doi:10.1002/adma.200700733)
5. Kim S, Sitti M, Xie T, Xia XC. 2009 Reversible dry micro-fibrillar adhesives with thermally controllable adhesion. *Soft Matter* **5**, 3689–3693. (doi:10.1039/B909885b)
6. Northen MT, Greiner C, Arzt E, Turner KL. 2008 A gecko-inspired reversible adhesive. *Adv. Mater.* **20**, 3905–3909. (doi:10.1002/adma.200801340)
7. Jeong HE, Kwak MK, Suh KY. 2010 Stretchable, adhesion-tunable dry adhesive by surface wrinkling. *Langmuir* **26**, 2223–2226. (doi:10.1021/la904290g)
8. Paretkar D, Kamperman M, Schneider AS, Martina D, Creton C, Arzt E. 2011 Bioinspired pressure actuated adhesive system. *Mater. Sci. Eng. C* **31**, 1152–1159. (doi:10.1016/j.msec.2010.10.004)
9. Nadermann N, Ning J, Jagota A, Hui CY. 2010 Active switching of adhesion in a film-terminated fibrillar structure. *Langmuir* **26**, 15 464–15 471. (doi:10.1021/la102593h)
10. Arul EP, Ghatak A. 2012 Control of adhesion via internally pressurized subsurface microchannels. *Langmuir* **28**, 4339–4345. (doi:10.1021/la204618u)
11. del Campo A, Greiner C, Arzt E. 2007 Contact shape controls adhesion of bioinspired fibrillar surfaces. *Langmuir* **23**, 10 235–10 243. (doi:10.1021/la7010502)
12. del Campo A, Greiner C. 2007 SU-8: a photoresist for high-aspect-ratio and 3D submicron lithography. *J. Micromech. Microeng.* **17**, R81–R95. (doi:10.1088/0960-1317/17/6/r01)
13. Bowden N, Brittain S, Evans AG, Hutchinson JW, Whitesides GM. 1998 Spontaneous formation of ordered structures in thin films of metals supported on an elastomeric polymer. *Nature* **393**, 146–149. (doi:10.1038/30193)
14. McDonald JC, Whitesides GM. 2002 Poly(dimethylsiloxane) as a material for fabricating microfluidic devices. *Acc. Chem. Res.* **35**, 491–499. (doi:10.1021/Ar010110q)
15. Gorb S, Varenberg M, Peressadko A, Tuma J. 2007 Biomimetic mushroom-shaped fibrillar adhesive microstructure. *J. R. Soc. Interface* **4**, 271–275. (doi:10.1098/rsif.2006.0164)
16. Hui CY, Jagota A, Lin YY, Kramer EJ. 2002 Constraints on microcontact printing imposed by stamp deformation. *Langmuir* **18**, 1394–1407. (doi:10.1021/La0113567)
17. Majumder A, Ghatak A, Sharma A. 2007 Microfluidic adhesion induced by subsurface microstructures. *Science* **318**, 258–261. (doi:10.1126/science.1145839)
18. Kroner E, Blau J, Arzt E. 2012 Note: an adhesion measurement setup for bioinspired fibrillar surfaces using flat probes. *Rev. Sci. Instrum.* **83**, 016101. (doi:10.1063/1.3675888)
19. Josse G, Sergot P, Creton C, Dorget M. 2004 Measuring interfacial adhesion between a soft viscoelastic layer and a rigid surface using a probe method. *J. Adhes.* **80**, 87–118. (doi:10.1080/00218460490276821)
20. Timoshenko SP, Gere JM. 1961 *Theory of elastic stability*, 2nd edn. New York, NY: McGraw-Hill.
21. Paretkar DR, Bartlett MD, McMeeking R, Crosby AJ, Arzt E. 2013 Buckling of an adhesive polymeric micropillar. *J. Adhes.* **89**, 140–158. (doi:10.1080/00218464.2013.731941)
22. Stark S, Begley M, McMeeking RM. In press. The buckling and post-buckling of fibrils adhering to a rigid surface. *J. Appl. Mech*. (doi:10.1115/1.4023107)
23. Timoshenko S, Woinowsky-Krieger S. 1959 *Theory of plates and shells*. New York, NY: McGraw-Hill.
24. Hui C-Y, Jagota A, Shen L, Rajan A, Glassmaker N, Tang T. 2007 Design of bio-inspired fibrillar interfaces for contact and adhesion: theory and experiments. *J. Adhes. Sci. Technol.* **21**, 1259–1280. (doi:10.1163/156856107782328362)
25. Peressadko A, Gorb SN. 2004 When less is more: experimental evidence for tenacity enhancement by division of contact area. *J. Adhes.* **80**, 247–261. (doi:10.1080/00218460490430199)
26. Varenberg M, Gorb S. 2008 Close-up of mushroom-shaped fibrillar adhesive microstructure: contact element behaviour. *J. R. Soc. Interface* **5**, 785–789. (doi:10.1098/rsif.2007.1201)
27. Spuskanyuk AV, McMeeking RM, Deshpande VS, Arzt E. 2008 The effect of shape on the adhesion of fibrillar surfaces. *Acta Biomater.* **4**, 1669–1676. (doi:10.1016/j.actbio.2008.05.026)
28. Carbone G, Pierro E, Gorb SN. 2011 Origin of the superior adhesive performance of mushroom-shaped microstructured surfaces. *Soft Matter* **7**, 5545–5552. (doi:10.1039/c0sm01482f)
29. Greiner C, Campo AD, Arzt E. 2007 Adhesion of bioinspired micropatterned surfaces: effects of pillar radius, aspect ratio, and preload. *Langmuir* **23**, 3495–3502. (doi:10.1021/la0633987)
30. Glassmaker NJ, Himeno T, Hui CY, Kim J. 2004 Design of biomimetic fibrillar interfaces: 1. Making contact. *J. R. Soc. Interface* **1**, 23–33. (doi:10.1098/rsif.2004.0004)
31. Kroner E, Paretkar D, McMeeking R, Arzt E. 2011 Adhesion of flat and structured PDMS samples to spherical and flat probes: a comparative study. *J. Adhes.* **87**, 447–465. (doi:10.1080/00218464.2011.575317)